remote sensing

MDPI

Article

Spatiotemporal Patterns of Evapotranspiration in Central Asia from 2000 to 2020

Xingming Hao [1,2,*], Xue Fan [1,2,3], Zhuoyi Zhao [1,2,3] and Jingjing Zhang [1,2,3]

[1] State Key Laboratory of Desert and Oasis Ecology, Xinjiang Institute of Ecology and Geography, Chinese Academy of Sciences, Urumqi 830011, China
[2] Akesu National Station of Observation and Research for Oasis Agro-Ecosystem, Akesu 843017, China
[3] University of Chinese Academy of Sciences, Beijing 100049, China
* Correspondence: haoxm@ms.xjb.ac.cn; Tel.: +86-991-7823056

Abstract: Evapotranspiration (*ET*) affects the dry and wet conditions of a region, particularly in arid Central Asia, where changes in evapotranspiration profoundly influence society, the economy, and ecosystems. However, the changing trends in and driving factors of evapotranspiration in Central Asia remain unclear. Therefore, we used estimated *ET* and reanalysis data to answer research questions. Our results showed that (1) potential evapotranspiration (*PET*) and *ET* showed a generally downward trend, in which *PET* and *ET* decreased in 37.93% and 17.42% of the total area, respectively. However, *PET* and *ET* showed opposite trends in 59.41% of the study area, mainly showing a decrease in *PET* and an increase in *ET*. (2) The absolute contribution rates of vegetation–human activity coupling factor (*VH*), *PET*, and precipitation (*P*) to *ET* were 43.19%, 40.02%, and 16.79%, respectively, and the *VH* was the main determiner of *ET*. (3) Transpiration (ET_c) dominated the change in *ET* in 56.4% of the region, whereas soil evaporation (ET_s) dominated the change in *ET* in the rest of the region. The coverage threshold that determines the dominant contributions of ET_c and *ETs* to *ET* was approximately 18–19%. Below this coverage threshold, the contribution rate of ET_s to *ET* exceeded that of ET_c and vice versa. In the context of global climate change, this study can provide scientific support for the restoration of water resources and sustainability evaluation of water resources.

Keywords: potential evaporation (*PET*); climatic factors; transpiration; soil evaporation

Citation: Hao, X.; Fan, X.; Zhao, Z.; Zhang, J. Spatiotemporal Patterns of Evapotranspiration in Central Asia from 2000 to 2020. *Remote Sens.* **2023**, *15*, 1150. https://doi.org/10.3390/rs15041150

Academic Editor: Conghe Song

Received: 26 October 2022
Revised: 15 February 2023
Accepted: 16 February 2023
Published: 20 February 2023

1. Introduction

Terrestrial evapotranspiration (*ET*) is a physical process closely related to factors including the atmosphere, vegetation, soil, and human activity. Changes in *ET* directly affect the water cycle and energy balance of the land surface, and profoundly affect water availability, food supply, and economic development [1,2]. In Central Asia (CA), owing to the inherently water-scarce and arid environment [3], variation in *ET*, particularly an increase, leads to significant challenges to the water supply [4]. As *ET* is sensitive to climatic factors [5,6], the CA region could show a trend of increasing *ET* and decreasing precipitation [7], and could face severe water shortages in the context of future climate change. Therefore, understanding the dynamic processes of *ET* and the driving factors in changing environments has significant implications for hydrology, ecological research, and socially sustainable development.

Accurately estimating *ET* is crucial to determining the changing trends and driving factors of *ET*. At present, *ET* is conventionally estimated by employing four methods: (1) direct observation by a lysimeter or flux system (*EC* method), which is currently the most accurate method to obtain site-scale *ET* data [8,9]. However, it is difficult for site-scale observations to meet the requirements of regional-scale research. (2) In research on agricultural water demand and irrigation decision-making, *ET* can be obtained by multiplying the reference crop evapotranspiration (also called potential evapotranspiration, *PET*) and crop

coefficient [10]. This method is effective for crops, but problems occur when it is applied to natural vegetation communities with mixed species, as the *Kc* coefficient (ratio of actual crop evapotranspiration to reference crop evapotranspiration) of natural vegetation cannot be effectively obtained. Moreover, studies have shown that the *Kc* coefficient could vary with changes in *PET* [11]. (3) In the field of hydrology, *ET* is typically estimated using the water balance method [12,13] based on sufficient hydrological observation data. The *ET* estimated in this manner is usually the total *ET* amount of a region, but low spatiotemporal resolution limits the application of the method. (4) Another effective approach is estimating *ET* using a surface energy balance (SEB) model based on remote sensing data [14,15]. Considering that *ET* has two main components, transpiration and soil evaporation, the community land model (CLM) [10] and two-source energy balance (TSEB) model [16] have been developed and applied to effectively partition these components.

Under the pressure of climate change and the discrepancy between water supply and demand, it is crucial to understand the driving mechanisms of *ET* variation to facilitate the formulation of sustainable water management policies. Generally, *PET* is highly correlated with *ET* and has the same value as *ET* in areas with ample water supply. Therefore, *PET* could be a key factor driving changes in *ET*. However, *PET* and *ET* often have a complementary relationship because of the spatial heterogeneity of the available water and energy conditions and the influence of vegetation processes [17]. Consequently, the main drivers of *ET* could differ in different regions. Studies have shown that, at the global scale, precipitation and catchment characteristics are dominant factors controlling the monthly and annual-scale variations of *ET*. However, in humid regions, the effect of *PET* on monthly *ET* variability is generally greater than that of precipitation or catchment characteristics [18]. In the arid regions of northwest China, precipitation is the main determining factor of *ET*, contributing 73% to the variation in annual *ET* in vegetated areas [6]. In addition, the coupling factors between rainfall and vegetation, and rainfall and *PET* significantly affect *ET* [19]. Furthermore, vegetation usually plays an active role in *ET* changes and dominates such changes in some regions. In the arid regions of China, an increase in vegetation dominates positive *ET* trends for shrubs, meadows, and steppe [6]. In the semi-arid Loess Plateau, revegetation contributes approximately 32% to the increase in *ET* [5], whereas in the Mekong River Basin of South Asia, vegetation greening accounts for 54.1% of the annual *ET* change [20].

The arid and semi-arid regions of CA cover an area of 5×10^6 km^2 [21], accounting for approximately 8.4% of the global arid region. In such a vast arid region, changes in *ET* inevitably have profound effects on water resources, ecosystems, human society, and the economy. However, the changing trend of *ET* and its driving factors in the arid CA region remain unclear. Current research shows a CA warming rate of 0.4 °C per decade over the past 30 years, which exceeds the Northern Hemisphere average of 0.3 °C per decade [21]. Generally, a temperature rise could lead to a significant increase in *PET*, implying an increase in *ET*. However, considering the complementary relationship between *PET* and *ET* [8,17], the changing trends in *PET* and *ET* might not be consistent. In addition, precipitation in arid regions is completely consumed by the evapotranspiration process. An increase in precipitation has direct positive effects on *ET*, but could have a negative effect on *PET* [4]. Therefore, in the context of climate change with warming and increased precipitation [21,22], the changing trends of *PET* and *ET* in CA, as well as the effect of *PET* on *ET* need to be investigated.

In addition to climatic factors, human activities often significantly affect natural systems and could even determine the evolution of regional microclimates and ecosystems in arid areas. For example, human activities have dominated the evolution of hydrological and ecological processes in the lower reaches of the Tarim River over the past century [23]. Furthermore, the recent Aral Sea crisis in the CA region is attributed to human activities [24,25]. Notwithstanding, information on the extent of the influence of human activity on *ET* remains insufficient. Therefore, we focused our analysis on the arid CA region and addressed three research questions through the estimated *ET* and employing reanalysis

data. The research questions pertain to (i) the spatiotemporal variation of *PET* and *ET* in CA; (ii) the contribution rate of *PET*, precipitation, vegetation status, and human activities to evapotranspiration; and (iii) the roles of transpiration and soil evaporation in *ET* trends.

2. Data and Methods

2.1. Study Area

CA is located in the hinterland of Eurasia, with a total land area of approximately 566.69 × 10^4 km^2. The coordinates of CA is between 46°–97°E and 34°–56°N, spanning six countries from east to west, namely, Kazakhstan (272.49 × 10^4 km^2), Kyrgyzstan (19.85 × 10^4 km^2), Tajikistan (14.31 × 10^4 km^2), Turkmenistan (48.81 × 10^4 km^2), Uzbekistan (44.74 × 10^4 km^2), and the Xinjiang region of China (166.49 × 10^4 km^2) (Figure 1). Influenced by land and sea location and the interaction between the westerly wind and the monsoon caused by the "pan-third pole" [26], precipitation in the study area is rare (about 200 mm/year), with huge regional variations. The annual average precipitation ranges from less than 30 mm (desert) to more than 1000 mm (mountain). Therefore, the demand of atmospheric evapotranspiration in this region is strong, and almost all the limited precipitation is consumed by evapotranspiration, thus, becoming a typical resource-water shortage region [27]. At present, under the influence of global climate change, the ranges of temperature rise and precipitation fluctuation in CA are higher than the global level, which has led to great variation of the hydrothermal conditions [27,28] and vegetation activities [29]. The change of these conditions directly results in the redistribution of water and heat flux between vegetation transpiration and soil evaporation.

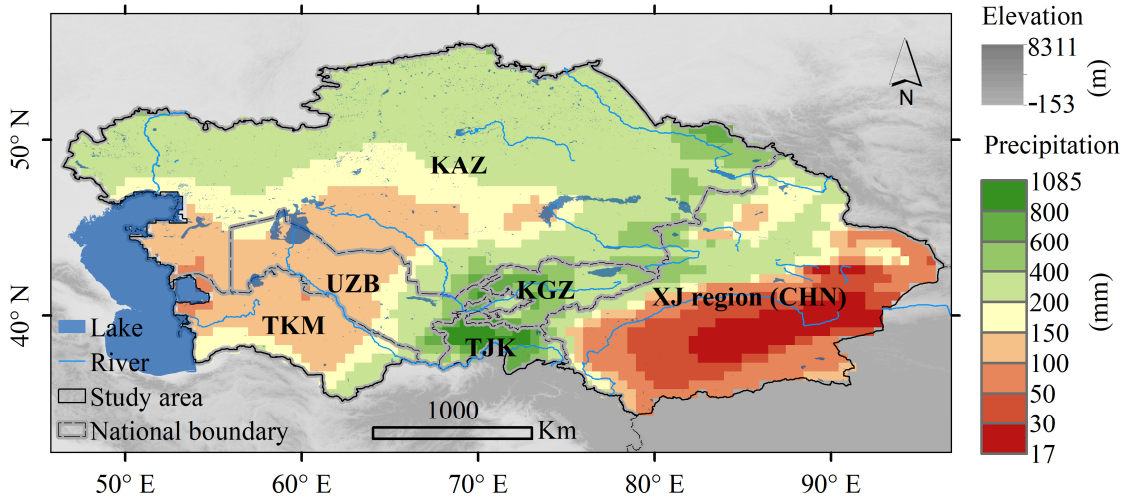

Figure 1. Basic geographic and precipitation information of the arid Central Asia.

2.2. Data Sources

In this study, *ET* was calculated based on remote sensing image data. The data used were the normalized vegetation index (NDVI), surface temperature (T_s), surface emissivity (E_s), surface albedo (A), and downward shortwave radiation (S_d). These data were downloaded from Moderate Resolution Imaging Spectrometer (MODIS) data products. The MOD13A2 dataset was selected for NDVI, with a spatiotemporal resolution of 1 km and 16 days. We selected T_s and E_s from the MOD13A2 dataset, with a daily spatiotemporal resolution of 1 km. The surface albedo data were selected from the MCD43A3 dataset, with a spatiotemporal resolution of 500 m, and the S_d data were from the Global Land Surface Satellite (GLASS) data provided by the University of Maryland team, with a spatiotemporal resolution of 1 day and 0.05°. The above datasets were for 2000–2020.

In addition, we used Famine Early Warning Systems Network (FEWS NET) Land Data Assimilation System (FLDAS) products during 2000–2020. Monthly net radiation, soil heat flux, air temperature, wind speed, atmospheric pressure, and air-specific humidity (con-

verted to relative air humidity) were used to calculate *PET*. The FLDAS monthly datasets, with a spatial resolution of 0.1°, were derived from the Noah version 3.6.1 land-surface model (LSM) (FLDAS_NOAH01_C_GL_M, FLDAS_NOAH01_CP_GL_M) (National Aeronautics and Space Administratio, Washington, DC, USA).

Precipitation data from 2000 to 2020 were derived from the European Centre for Medium-Range Weather Forecasts (ECMWF) Reanalysis V5 (ERA5) land monthly averaged data, with a spatial resolution of 0.1°. Elevation data were derived from 1 km global digital elevation data provided by the US National Oceanic and Atmospheric Administration. The land cover data were chosen from the 2016 land cover data produced by the European Space Agency Climate Change Initiative (ESACCI) with a spatial resolution of 300 m. According to the IPCC land classification, the land cover data were reclassified into eight categories; forest, shrub, grassland, sparse vegetation (coverage less than 15%), urban land, irrigated cropland, rain fed cropland, and bare land.

All these data were processed by ArcGIS Desktop V10.3 (Environmental Systems Research Institute Inc., Redlands CA, USA) and MATLAB software (R2013a, MathWorks, Natick, MA, USA).

2.3. Methods

2.3.1. Algorithm of ET and PET

We used the Priestley–Taylor diurnal land surface temperature range (PT-DTsR) model proposed by Yao and coworkers [16] to estimate *ET* based on the MODIS datasets. This model partitions evapotranspiration (*ET*) into four components; soil evaporation (ET_S), vegetation transpiration (ET_C), canopy interception (ET_i), and wet soil surface evaporation (ET_{ws}). The Priestley–Taylor equation was used to calculate the potential value of each evapotranspiration component. Subsequently, environmental limiting factors (e.g., soil moisture limit and temperature limit) were used to correct the potential value and obtain the actual value of each component.

The classic Penman–Monteith–United Nations Food and Agriculture Organization (PM–FAO) method [30,31] was used to estimate *PET*. The data required for the calculation mainly derive from FLDAS monthly data.

2.3.2. Attribution of ET Changes

Generally, *PET* refers to evaporative capacity. This variable combines several meteorological factors, such as air temperature, wind speed, and radiation. Under ideal conditions, the *PET* trend is highly consistent with actual evapotranspiration, and variation in *PET* represents change in *ET*.

As the influence of precipitation is not considered in potential evapotranspiration, we presumed well-growing vegetation underlying the surface. In practice, precipitation and vegetation are two crucial variables that affect actual evapotranspiration. In arid regions, where water supply is insufficient, natural precipitation at annual scale is eventually consumed directly or indirectly through evapotranspiration. Therefore, changes in annual precipitation in arid regions directly contribute to annual-scale changes in *ET*. Considering vegetation is often disturbed by human activities, coupling between vegetation and such activities is another important and most complex factor in actual evapotranspiration. In summary, the main influencing factors in the evapotranspiration trend can be summarized in three aspects; evaporation capacity, water supply, and the coupling factor between vegetation and human activities. This relationship is expressed mathematically as follows:

$$\Delta ET = \Delta ET_{pet} + \Delta ET_p + \Delta ET_{vh} \quad (1)$$

where ΔET is the variability of *ET* over several years; ΔET_{pet} is the variability of *ET* caused by *PET*, expressed by the linear slope of annual *PET* over the last 20 years; and ΔET_p is the variability of *ET* caused by changes in precipitation. Based on the assumption that all precipitation in arid regions is consumed by evapotranspiration, ΔET_p is the linear slope of annual precipitation over the last 20 years. ΔET_{vh} represents the variability of *ET* caused

by changes in vegetation and human activity, and its value can be solved by the inverse operation of the above formula.

The contribution rate of each element to *ET* is estimated using the following formula:

$$\varepsilon_{pet} = {}^{\Delta ET_{pet}}/(|\Delta ET_{pet}| + |\Delta ET_{p}| + |\Delta ET_{vh}|) \times 100\% \quad (2)$$

where ε_{pet} represents the contribution rate of *PET* to *ET*. Similarly, the contribution rate of precipitation and the coupling factor of vegetation and human activities to *ET* can be calculated and recorded as ε_{p} and ε_{vh}, respectively.

2.3.3. Trend Analysis

In trend analysis, the Sen Slope estimation is conventionally used to calculate the trend value and, subsequently, the Mann–Kendall (MK) method is used to judge the significance of such a trend [32,33].

3. Results

3.1. Changing Trend of ET and PET

Both potential evapotranspiration and actual evapotranspiration showed significant spatiotemporal variations. The *PET* in the study area ranged from 610 to 4348 mm, with a multi-year average *PET* of 2215 mm. An obvious *PET* decreasing trend is observed along with an increase in latitude. However, in an area with similar latitudes, *PET* also shows a significant downward trend along with an increase in altitude, similar to the changing trend of temperature (Figure 2a). The annual *ET* in CA ranges from 0 to 1038 mm, with a multi-year average of 138 mm. These figures are consistent with the basic characteristics of water shortages, sparse vegetation, and substantial distribution of bare land in arid regions. In terms of spatial variation, *ET* does not show variation with latitude but does show a tendency for high *ET* values in high-altitude areas, which is the opposite of the performance of *PET* (Figure 2c). The relationship between *ET* and elevation mainly depends on vegetation conditions. In arid regions, natural vegetation growth in mountainous areas is often superior to that in the plains. Therefore, the spatial variation of *ET* is highly consistent with the spatial variation of NDVI, tending to show higher values in mountains, oasis farmland, and vegetation areas, as well as river systems.

Over the past 20 years, *PET* and *ET* have shown diverging trends (Figure 2b,d). In the entire CA, *PET* shows a downward trend in 85.24% of the area, with 37.93% of the area showing a significant downward trend. As regards to the increasing trend, *PET* shows such a trend in only 14.76% of the total area, with 1.69% of the area showing a significant increasing trend. The spatial variation of *PET* shows a downward trend in the central and eastern regions of CA, with a significant decrease in the eastern Xinjiang region and the northern high-latitude region (Figure 2b). Compared with *PET*, *ET* shows a downward trend in only 51.92% of the area, with a significant downward trend in 17.42% of this area. In the remaining 48.08% of the area, *ET* shows an increasing trend, with a significant increasing trend in 16.43% of the area. In the eastern and central regions of CA, a more obvious increasing trend in *ET* is shown, with a decreasing trend in the western region. This trend is the opposite of the spatial distribution characteristics of *PET* trends (Figure 2d). The transition matrixes of different *PET* and *ET* trends also show the robust opposite trends of *PET* and *ET* (Figure 2e). The area where *PET* and *ET* maintain an increasing trend accounts for only 1.51% of the total study area, whereas a decreasing trend accounts for 39.07% of the total area. In contrast, in the remaining 59.41% of the area, *PET* and *ET* show opposite trends. In 13.22% of the total area, *PET* increases and *ET* decreases, whereas *PET* decreases and *ET* increases in 46.19% of the total area.

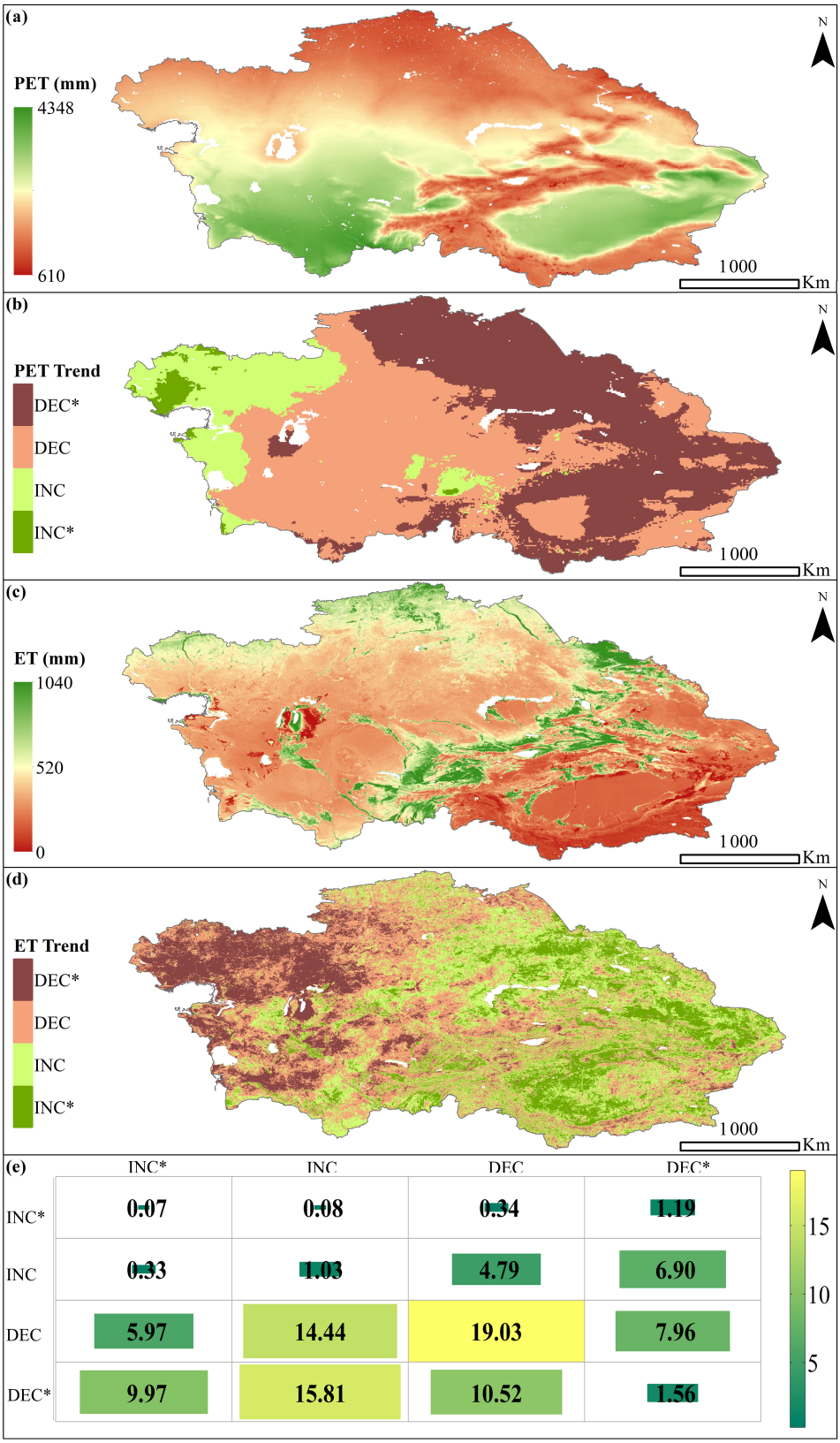

Figure 2. Spatiotemporal changing trends of annual *PET* and *ET* during 2000–2020. (**a**,**b**) Multi-year average *PET* and its changing trend over the same period. (**c**,**d**) Multi-year average *ET* and its changing trend during the same period. (**e**) Area transfer matrix between *PET* and *ET*, with different change trends. The characters "DEC" and "INC" mean the decrease and increase trends, respectively, and the symbol "*" shows that the change trend reaches the significant level (95% confidence).

3.2. Attribution of ET Trend

The variation in *ET* not only depended on the changing trend of *PET* but also was affected by precipitation, vegetation conditions, and human activities. In particular, the coupling factor between vegetation and human activity (*VH*) was the main determinant of the change in *ET*. The contribution rate of *VH* to *ET* change was positive in 82.64% of the entire CA region, with an average contribution rate of 45.62%. In the remaining 17.36% of the region, the contribution rate of *VH* to *ET* change is negative, with an average contribution rate of −31.64% (Figure 3a). Further, *PET* has a significant effect on *ET*, with its contribution to *ET* being second only to that of *VH-PET*. The contribution rate of *PET* to *ET* change in 22.33% of the total area is positive, with an average of 34.83%. In the remaining 77.67% of the area, the contribution rate of *PET* to *ET* change is negative, with an average value of −41.38% (Figure 3b). The average contribution rate of precipitation to *ET* is the lowest. In 36.71% of the study area, the contribution rate of precipitation to *ET* is positive, with an average rate of 10.29%. In the remaining 63.29% of the area, variation in precipitation leads to a decrease in *ET*, with an average contribution rate of −20.34% (Figure 3c). Overall, at a regional scale, the average contribution rates of *VH*, *PET*, and *P* to *ET* (considering positive and negative effects) are 32.21%, −24.26%, and −9.07%. The average absolute contribution rates are 43.19%, 40.02%, and 16.79%, respectively. In addition, the standard deviations of the contribution rates of *VH*, *PET*, and *P* to *ET* are 54.73, 34.83, and 26.40, respectively, indicating that *VH* has the most significant effect on *ET*, followed by *PET*, whereas precipitation is a relatively stable factor. The absolute value of the contribution rate of *VH* is the main factor leading to *ET* change, regardless of the effect being positive or negative.

From the perspective of different land-use types (Figure 4c), from Crop I, urban land, bare land, Crop R, forestry, shrubs, and grassland to sparse vegetation, the absolute value of the contribution rate of *VH* to *ET* decreases from 51.19% to 40.54%. The absolute values of the contribution rate of *PET* and precipitation to *ET* show a slight fluctuation and increase, with no significant negative correlation between them ($R^2 = 0.44$, $p < 0.05$). The absolute value of the contribution rate of *PET* to *ET* is between 32.32 and 44.45%, of which *PET* has the highest contribution rate to Crop R and the lowest to Crop I. The absolute value of the contribution rate of precipitation to *ET* is between 11.85 and 22.65%, of which *P* has the lowest contribution rate to Crop R and the highest to sparse vegetation.

The contribution rate of *PET* to changes in *ET* was highest in low-coverage areas. Along with an increase in vegetation coverage, the contribution rate of *PET* generally showed an obvious downward trend; however, with intense fluctuation in high-coverage areas (mountainous areas with high-vegetation coverage and irrigated agricultural areas). The contribution rate of precipitation to *ET* increased with an increase in coverage, but the contribution rate tended to be stable when the coverage exceeded 30%. The contribution of *VH* to *ET* along the coverage gradient shows a relatively gradual increasing trend (Figure 4b). Similar to the contribution rate of *PET* to *ET*, the contribution rates of *P* and *VH* show substantial fluctuations in high-coverage areas.

Along the altitude gradient, the contribution rate of *PET* showed a trend of initially slowly decreasing and then increasing, and *PET* often had the lowest contribution rate at altitudes of approximately 2050–3500 m. The contribution rate of *VH* to *ET* reached a maximum at an altitude of approximately 1000 m, after which it started to decrease with the increase in elevation. The contribution rate of *VH* to *ET* increased with an increase in elevation above 4000 m. The contribution rate of *P* to *ET* remained low at an altitude of approximately 1000 m, increased with an increase in altitude, and significantly decreased when the altitude exceeded 4000 m (Figure 4a). The contribution rate of precipitation to *ET* along the altitude gradient was negatively correlated with *PET* ($R^2 = 0.42$, $p < 0.01$) and *VH* ($R^2 = 0.61$, $p < 0.01$).

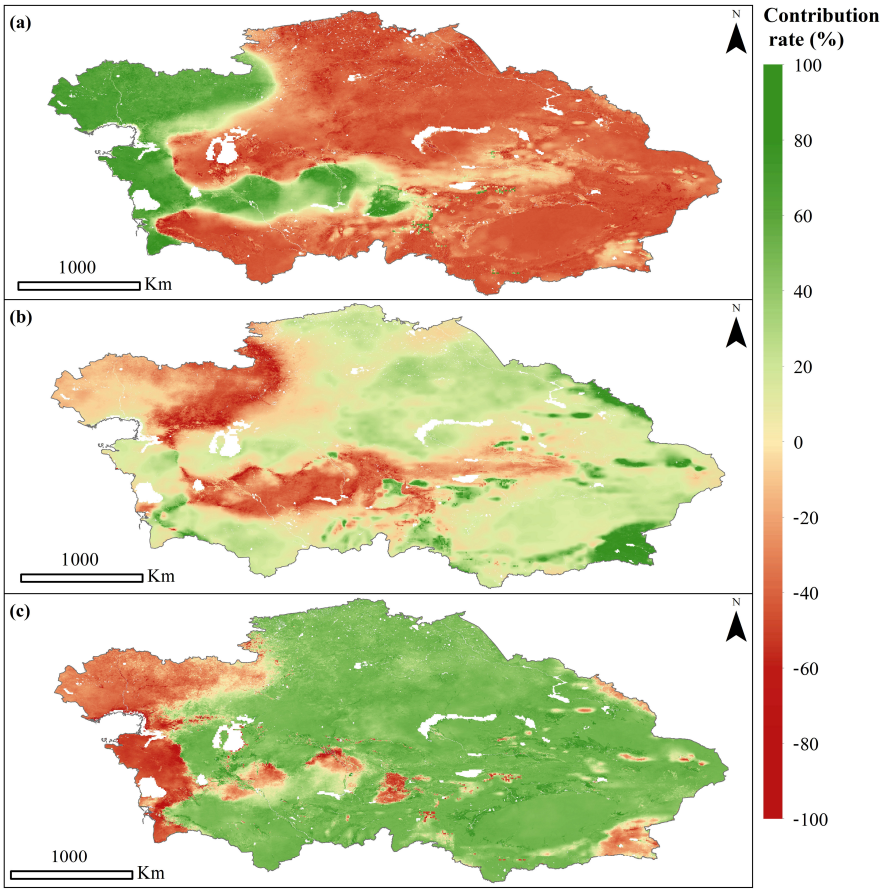

Figure 3. Spatial variation in the contribution rates (%) of annual *PET* (**a**), *P* (**b**), and *VH* (**c**) to annual *ET* from 2000 to 2020.

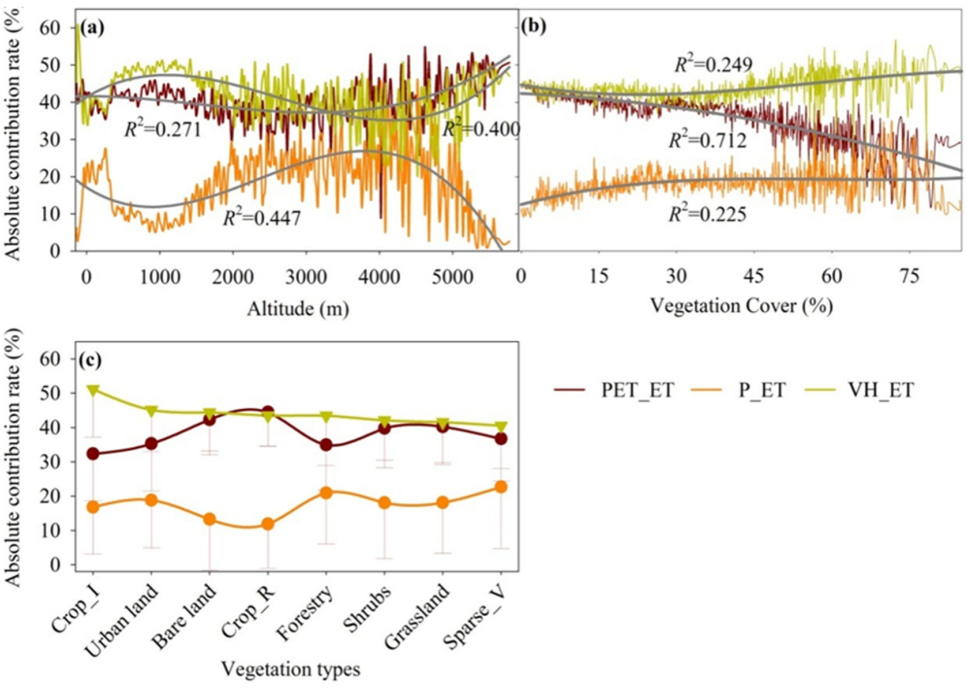

Figure 4. Changing trend of absolute contribution rates of annual *PET*, *P*, and *VH* to *ET* along altitude (**a**) and vegetation cover (**b**) grades, and that in different vegetation types (**c**). In panel (**c**), the Crop I and Crop R present the irrigated and rain-fed cropland, and Sparse V is the sparse vegetation (coverage less than 15%).

3.3. Contribution of Soil Evaporation and Transpiration to ET Change

The contribution rates of ET_C and ET_S to ET are similar, but with obvious regional differences (Figure 5). In the study area, the average contribution rates of ET_C and ET_S to ET variation are 49.62% and 50.38%, with ET_C dominating the change in ET in 56.4% of the area, and ET_S dominating in the rest of the area. The contribution of ET_C to ET change is highly correlated with vegetation coverage, and the contribution rate rapidly increases along with an increase in vegetation coverage. The contribution rate of ET_C to ET change tends to be smooth when the vegetation coverage exceeds 40%. The changing trend of the contribution rate of ET_S to ET with vegetation coverage is the opposite of that of ET_C. The coverage threshold that determines the dominant contributions of ET_C and ET_S to ET is approximately 18–19%. Below this coverage threshold, the contribution rate of ET_S to ET is greater than that of ET_C, and the lower the coverage, the stronger is the dominance of ET_S. However, when the coverage exceeds this threshold, the contribution rate of ET_C to ET is greater than that of ET_S, and the higher the coverage, the greater is the contribution rate of ET_C (Figure 5a).

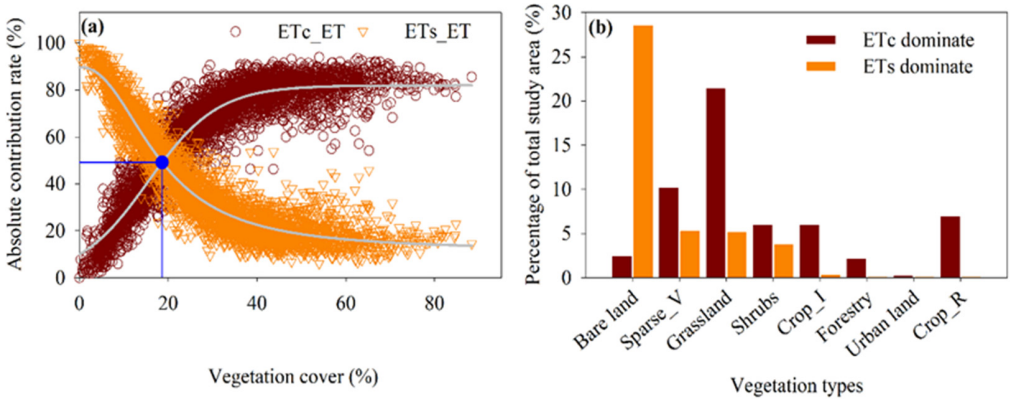

Figure 5. Contribution rate (%) of ET_C and ET_S to ET from 2000 to 2020. (**a**) Contribution rate of ET_C and ET_S to ET along the vegetation cover gradient. (**b**) Percentage of area where ET_C and ET_S dominate ET variation in the total study area under different vegetation types. In panel (**b**), the crop I and crop R represent the irrigated and rain-fed croplands, respectively, and sparse V indicates sparse vegetation.

Among the different land-use types, ET_S almost completely dominated the changing trend of ET on bare land, being dominant in 92.25% of the total bare land area. Moreover, in areas of sparse vegetation, shrubs, grassland, and urban land, ET_S influenced ET changes, being dominant in 33.99%, 38.49%, 19.35%, and 16.66% of the total area of the above land-use types, respectively. As regards forest and farmland types, ET_C dominated the changing trend of ET, being dominant in more than 95% of the area. Generally, except for bare land, ET_C is the dominant factor in ET change in different land-use types, being dominant in 99.51%, 96.98%, 95.10%, 83.34%, 80.65%, 66.01%, and 61.51%, respectively, of rain fed cropland, forestry, irrigated cropland, urban land, grassland, sparse vegetation, and shrub areas (Figure 5b).

4. Discussion

4.1. Driving Forces of ET Variation in Arid Region

Generally, variations in ET are influenced by climatic factors, vegetation, and human activities. In the humid areas of mainland China, the contribution of climate variation to ET change is higher than 90%, and the contribution of vegetation greening is lower than 10% [34]. Among the climatic factors; precipitation, air temperature, wind speed, and relative humidity have obvious effects on the evaporation process [35]. Current research shows that, from regional to global scales, precipitation is the most important climatic factor influencing ET [6,18,36]. However, vegetation factors could make a more significant contri-

bution to *ET* in some areas [6]. For example, re-vegetation of the Loess Plateau (quantified by an increase in NDVI) contributed approximately 32% to the increase in *ET* [5], whereas vegetation greening accounted for 54.1% of the annual *ET* variation in the Mekong River Basin [5,20]. Our study showed that climate variation dominated the inter-annual variation in *ET* in the arid regions of CA. The contribution of evaporation capacity, represented by *PET* to *ET*, was far greater than that of precipitation, with the average absolute contribution rates of the two factors being 40.02% and 16.79%, respectively. However, the average absolute contribution rate of the coupling factor of *VH* to *ET* was also high at 43.19%. This indicates that coupling factors of *VH* remain the most important influence on *ET* among the three elements [evaporation capacity, water supply (precipitation), and coupling between *VH* activities] in the arid region of CA.

Human activity is one of the most important factors affecting the water cycle. On the one hand, it changes the runoff process and total land water storage [37,38], and on the other hand, it directly or indirectly affects *ET* by altering the local hydrological and vegetation processes [39,40]. However, quantitatively assessing the effect of large-scale human activities on *ET* remains a challenge. This study tries to estimate the approximate spatial characteristics and degree of influence of human activities on *ET* based on the following workflow (Figure 6). In areas with no or sparse vegetation, the coupling factor of *VH* should be dominated by human activities. In such areas, human activities affect the groundwater level and soil moisture by changing the surface runoff process, groundwater pumping for irrigation, farmland drainage, and other events, thereby affecting the *ET* process. Here, we set the proportion of ET_S to *ET* at higher than 90% to represent areas with no or sparse vegetation. Therefore, the contribution rate of *VH* may be understood as that of human activities in these areas. Thus, human activities could dominate *ET* variation in 34.39% of the total CA area, and the average absolute contribution rate of that was approximately 43.74% (Figure 6a). In the remaining 65.61% of areas with vegetation activity, we set the threshold for the contribution rate of human activities to NDVI at greater than 50% to quantify the influence of human activities on *ET* (the estimation method is shown in Appendix A). The area where human activities could be dominant comprises 32.70% of the total area, and the absolute average contribution rate of human activities to *ET* is at least 32.97% (Figure 6b).

Although this study can roughly distinguish the impact of human activities on *ET*, there is still some uncertainty in this analytical framework. In an area with ET_S greater than 90% of *ET*, the contribution of human activities could be overestimated because the influence of vegetation is not excluded, although the vegetation is extremely sparse. Underestimation could occur in the remaining areas, as only the indirect contribution of human activities to *ET* is considered through a direct effect on *NDVI*, whereas the possible effect of direct human activities on *ET* is not considered. Nevertheless, it is inferred that the contribution rate of *VH* to *ET* in the arid region of CA may be dominated by the contribution rate of human activities. The dominant area of human activities accounts for approximately 67% of the total area, and the average absolute contribution rate is between 32% and 43%.

The estimated contribution rate of human activities to *ET* change in this study is within the range of the estimations in the temperate monsoon and northwest arid regions of China (12–45.54%) [41,42]. Moreover, our estimation was consistent with those in the Aral Sea basin of Central Asia, where the contribution rate of human activities to *ET* changes was 45.54% [43]. While in the Aksu River basin in the Xinjiang region of Central Asia, human activities can explain more than 80% of *ET* changes in the vegetation system [44]. The above results mean that in the arid region of Central Asia, human activities may be the main driving factor leading to *ET* changes, and its role is often higher than that of precipitation. Furthermore, the impacts of human activities on *ET* may be less affected by local water conditions.

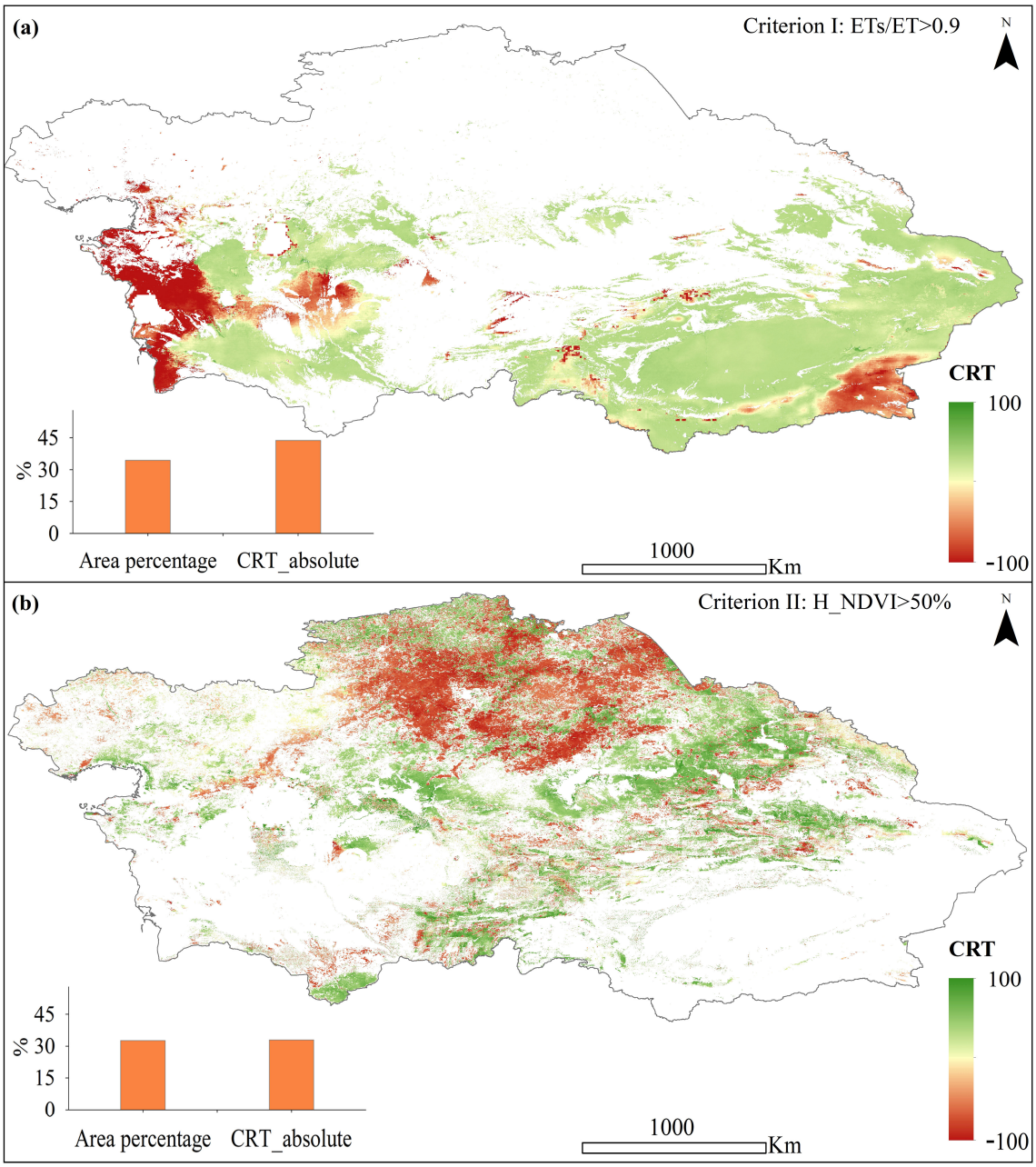

Figure 6. Contribution rate of human activities to *ET*, distinct from the contribution rate of *VH* coupling factors to *ET*. (**a**) Contribution rate of human activities to *ET* in areas with no or extremely weak vegetation; (**b**) Contribution rate of human activities to *ET* in other areas where human activities dominate the NDVI. The histogram in panels (**a**,**b**) shows the area percentages where human activity dominates *ET* change and the average absolute contribution rate of human activity to *ET* in the area where human activity dominates the contribution rate of the *VH* coupling factor to *ET*.

The results of typical regions in the study area also show that the analysis framework proposed in this study is a robust method. For example, owing to the intensification of human activities, especially agricultural activities, the 321 km river course in the lower reaches of the Tarim River was cut off for several years (1982–2000), groundwater level significantly decreased, and vegetation was severely degraded [23]. Since 2000, a sustainable ecological water conveyance project has been carried out in the lower reaches of the Tarim River, and the vegetation in the lower reaches has been restored [40]. As a result, *ET* in this region has shown a significant increase trend. The absolute contribution rate of human activities to *ET* is as high as 50%, higher than that of *PET* (47.32%) and precipitation (2.68%).

In the plains-desert area of the whole Tarim River basin, owing to the need to guarantee the ecological water demand of rivers and natural vegetation which has arisen in the past 10 years, as well as the expansion of irrigation areas and the impact of other projects [45,46], human activities have always been the greatest factor affecting the natural system in the region. Our assessment results also showed that the absolute contribution rate of human activities to *ET* in this region is as high as 48.77%. In addition, irrigation agriculture in CA is strongly affected by human activities, so the absolute contribution rate of human activities to *ET* is 37.16% in irrigated crop land. At the same time, owing to the demands of water supply of irrigated crop land, the variation of evaporation capacity is another key factor contributing to *ET*. In this regard, this study also successfully detected that the absolute contribution rate of *PET* to *ET* is 32.32%, which is second only to the impact of human activities.

4.2. Effects of PET on ET

Research regarding the effects of climatic factors on *ET* often focuses on the influence of specific meteorological elements, such as temperature, precipitation, wind speed, radiation term, and sunshine time [6,19]. However, analysis results could contain uncertainty owing to a probable autocorrelation between these meteorological factors. Therefore, *PET*, as a comprehensive index combining several meteorological elements, could represent regional evaporation capacity and climatic effects on *ET*, with the exception of precipitation. Generally, an increase in *PET* indicates an increase in *ET*, and this relationship is widely used in estimating crop water requirements [47]. Our research showed a positive relationship between *PET* and *ET* in 40.59% of the CA region. However, this positive relationship is not universal. Our study also showed that *PET* and *ET* had opposite trends in 59.41% of the total study area (Figure 2e). This finding could be mainly ascribed to the combined effects of precipitation, vegetation, and human activities. In areas with high annual precipitation and low temperatures, vegetation grows well, vegetation coverage is high, and it has a larger ET_C, often presenting the paradoxical phenomenon of *PET* and *ET*, and vice versa. In our study, the paradox between *PET* and *ET* mainly manifested as a decrease in *PET* and an increase in *ET*. In the context of climate change, the declining trend of *PET* could be ascribed to an increase in temperature [47], inhibiting the trend of promoting *PET* increase through temperature rise. In addition, other factors, such as wind speed, significantly affect *PET*. In the arid region of northwest China, which is the eastern part of CA, the decline in wind speed dominates the decline in *PET* [35,48].

4.3. Effects of Soil Evaporation and Mitigation Measures

Water is limited for the evaporation process in most of the CA region, except in several mountainous areas where the water conditions are sufficient. Water conditions determine evapotranspiration and the growth and development of natural vegetation; however, the sparse vegetation in the region leads to severe loss of soil evaporation. In our study, total soil evaporation accounted for 56.51% of total evapotranspiration. Artificial vegetation (farmland), natural vegetation, and bare land accounted for 13.48%, 55.03%, and 31.49% of the total study area, and contributed 15.53%, 54.34%, and 30.13% of the total soil evaporation, respectively (Figure 7). Artificial vegetation showed the highest contribution rate to soil evaporation in terms of the contribution rate per unit area.

The water-energy-food-ecology system is particularly vulnerable in CA, and the available water resources cannot meet the demand for the expansion of arable land. For example, in the Tarim Basin, the proportion of agricultural water consumption of total water consumption has reached 95%, with prominent overutilization of water resources [47]. Accordingly, if soil evaporation of existing farmlands could be reduced, the utilization rate of water resources could be significantly improved. According to our preliminary calculation results, soil evaporation related to rain-fed agriculture and irrigated agriculture was equivalent to 42.7% and 75.42% of transpiration, respectively. Measures to reduce soil evaporation could effectively expand the planting area, particularly for irrigated farmland.

Referring to the successful experience of irrigated agriculture in Xinjiang, China, technical measures such as drip irrigation and film mulching could be effective ways to improve the current water resource utilization efficiency and reduce wasteful soil evaporation.

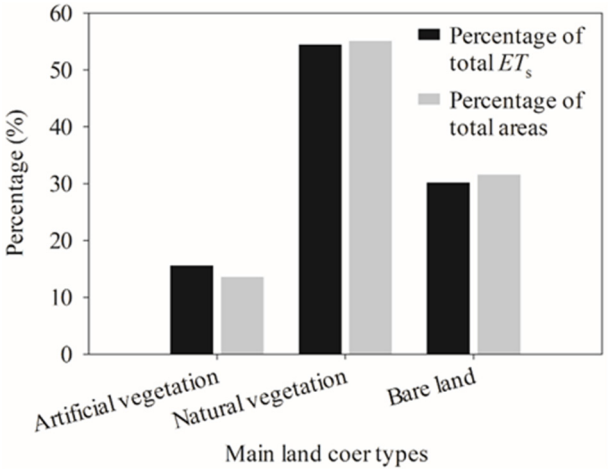

Figure 7. Percentage of artificial vegetation (farmland), natural vegetation, and bare land in the total study area, and the percentage of ET_S in ET in three land cover types (artificial vegetation, natural vegetation, and bare land).

5. Conclusions

Both *PET* and *ET* exhibited significant spatial and temporal variabilities. Over the past 20 years, *PET* and *ET* have generally shown a downward trend, but *ET* had a weaker downward trend and a stronger increasing trend than *PET*. In 59.41% of our study area, the changing trends of *ET* and *PET* showed contradictory trends.

The average absolute values of the contribution rates of *VH*, *PET*, and *P* to *ET* were 43.19%, 40.02%, and 16.79%, respectively. The contribution rate of *VH* coupling elements dominated the *ET* changes in CA regions. In addition, the contribution rates of ET_C and ET_S to *ET* were comparable, although regional differences were observed. Overall, except for bare land, ET_C was the dominant factor in *ET* in the various land-use types. The contribution rates of ET_C and ET_S to *ET* change were highly correlated with the vegetation coverage. The coverage threshold determining their dominance was approximately 18–19%. Below this coverage threshold, the contribution rate of ET_S to *ET* was greater than that of ET_C, and vice versa.

The data required by the analysis method proposed in this study are easy to obtain and the calculation process is simple, and it should, therefore, have high applicability in other regions. However, the impact of human activities and natural factors on *ET* is complex, and it is often difficult to partition the individual effects. Thus, this study can only give an approximate estimation of the impact of human activities on *ET*. As pointed out, our research method may overestimate the impact of human activities on *ET* in areas with sparse vegetation, while the opposite may occur in areas with lush vegetation. Therefore, a more accurate assessment method based on biological and physical processes is still required and needs to be addressed in future studies.

The driving factors of *ET* are the key issues of the water-energy-food-ecology system. Insightfully revealing the contribution of *VH*, *PET*, and *P* to *ET* would help to elucidate the influencing factors and driving mechanisms of *ET* under future climate change conditions, improve the efficiency of utilizing water resources, and ensure ecological and water security.

Author Contributions: All authors made significant contributions to this study. Conceptualization, X.H.; methodology, X.F.; data curation, Z.Z.; writing—original draft preparation, X.H.; formal analysis, X.F. and Z.Z.; writing—review and editing, X.H. and J.Z.; project administration, X.H.; funding acquisition, X.H. All authors have read and agreed to the published version of the manuscript.

Funding: This research was supported by the Natural Science Foundation of Xingjiang Province of China (No.: 2022D01E02).

Data Availability Statement: The MODIS data were downloaded from the website "National Aeronautics and Space Administration" (https://ladsweb.modaps.eosdis.nasa.gov/, accessed on 5 July 2022). The FLDAS monthly datasets, with a spatial resolution of 0.1°, were derived from the Noah version 3.6.1 land-surface model (LSM) (FLDAS_NOAH01_C_GL_M, FLDAS_NOAH01_CP_GL_M). The precipitation data were selected from the ERA5 dataset (https://cds.climate.copernicus.eu/cdsapp#!/dataset/reanalysis-era5-land-monthly-means?tab=overview, accessed on 20 July 2022). The elevation data were provided by the National Oceanic and Atmospheric Administration (https://www.ngdc.noaa.gov/mgg/topo/DATATILES/elev/, accessed on 17 August 2022). Land cover data were chosen from the 2016 land cover data produced by the European Space Agency Climate Change Initiative(ESACCI) (https://cds.climate.copernicus.eu/cdsapp#!/dataset/satellite-land-cover?tab=form, accessed on 20 August 2022).

Acknowledgments: We want to thank the editor and anonymous reviewers, whose comments have helped to improve the manuscript substantially.

Conflicts of Interest: The authors declare that they have no known competing financial interest or personal relationships that could have appeared to influence the work reported in this paper.

Appendix A

a. *ET* estimation and validation

This study estimated *ET* by using the modified satellite-based Priestley–Taylor algorithm [16]. This model is based on the PT-JPL model [49], and uses the apparent thermal inertia (ATI) instead of relative humidity (RH) and water vapor pressure deficit (VPD) to calculate soil moisture constraints. The modified algorithm simplifies the calculation process and reduces data requirements, which can well overcome the lack of ground data in CA [50]. This model partitioned evapotranspiration (*ET*) into four components: soil evaporation (ET_s), vegetation transpiration (ET_c), canopy interception (ET_i), and wet soil surface evaporation (ET_{ws}). The calculation formulas for the above components and variables are shown in Table A1.

Considering that using data from different data sources will bring uncertainty to *ET* simulation results, this study uniformly uses MODIS data to estimate *ET*. For the acquisition of air temperature (T_a), we took T_a, NDVI, T_s, and DEM as input variables, and performed a linear regression estimation based on the measured temperature at the site, thus obtaining the Equation (A1):

$$T_a = 0.87 \times T_s + 3.03 \times NDVI - 0.008 \times DEM + 35.14 \quad \text{(A1)}$$

Table A1. Model parameters and equations.

Parameter	Description	Equation
ET	Evapotranspiration	$ET_s + ET_c + ET_i + ET_{\mathrm{ws}}$
ET_c	Vegetation transpiration	$(1 - f_{wet}) f_v f_T \alpha \frac{\Delta}{\Delta+\gamma} R_{nc}$
ET_s	Soil evaporation	$(1 - f_{wet}) f_{sm} \alpha \frac{\Delta}{\Delta+\gamma} (R_{ns} - G)$
ET_i	Vegetation interception evaporation	$f_{wet} \alpha \frac{\Delta}{\Delta+\gamma} R_{nc}$
ET_{ws}	Wet soil surface evaporation	$f_{wet} \alpha \frac{\Delta}{\Delta+\gamma} (R_{ns} - G)$
f_v	Fraction of green vegetation in the scene	$\frac{NDVI - NDVI_{\min}}{NDVI_{\max} - NDVI_{\min}}$
f_T	Plant temperature constraint	$\exp\left[-\left((T_a - T_{opt})/T_{opt}\right)^2\right]$
f_{sm}	Soil moisture constraint	$(\frac{1}{DT})^{DT/DT_{\max}}$
f_{wet}	Relative surface wetness	${f_{sm}}^4$
Lu	Upward long wave radiation	$\varepsilon_s \sigma (T_s + 273.15)^4$
L_d	Downward long wave radiation	$(1 + 0.26\,\mathrm{n}) \varepsilon_a \sigma (T_a + 273.15)^4$
ε_a	Atmospheric emissivity	$1 - 0.261 \cdot \exp[-7.77 \times 10^{-4} \times (T_a + 0.15)^2]$
R_n	Net radiation	$S_d(1 - A) + \varepsilon_s L_d - L_u$
R_{nc}	Net radiation to the vegetation	$R_n f_v$
R_{ns}	Net radiation to the soil	$R_{ns} = R_n(1 - f_v)$

In the above formulae, T_a represents the air temperature, T_s represents the surface temperature, T_{opt} represents the optimum temperature (25 °C), A is the surface albedo, and NDVI is the normalized vegetation index. Δ is the slope of the saturated vapor pressure curve (kPa/°C); γ is the psychrometric constant (0.066 kPa/°C) and DT is the diurnal temperature range, DT_{max} = 60°; n is the cloudiness varying from 0 to 1 and is set as an invariant constant (0.5) in this paper; ε_s is the surface emissivity; σ is the Stefan–Boltzmann constant (5.67 × 10^{-8} W m^{-2} K^{-4}); S_d is the surface downward shortwave radiation (W/m^2).

The modified satellite-based Priestley–Taylor algorithm used in this study has been demonstrated to be effective in estimating *ET* under large-scale environmental gradients [16,50]. Furthermore, compared with the PM-mod model [51] and the PML model [52], this model has significant advantages in simulating *ET* temporal changes in China [50].

In addition, we verified the estimation results of this study with flux observation data (Akesu and Fukang sites) and simulation data from PML_V2 model [53]. On the site scale, the determination coefficient (R^2), root mean square error (*RMSE*), mean absolute percent error (*MAPE*), and Nash-Sutcliffe efficiency coefficient (*NSE*) between the simulated and measured *ET* values were 0.88, 9.68 mm, 17.24%, and 0.85, respectively (Figure A1a). Although the estimated monthly evapotranspiration is often low, the simulated and measured data are in good agreement over time.

Research has verified that the data of PML_V2 (with a spatiotemporal resolution of 0.05°and per year) has good accuracy [53,54]. Therefore, this study compared the annual *ET* data estimated in this study with the PML_V2 simulation data. The R^2, RMSE, MAPE, and *NSE* between the estimations and values of PML_V2 model were 0.85, 60.70 mm, 16.90%, and 0.78, respectively (Figure A1b). Compared with the PML_V2 data, although the data simulated in this study still has a certain degree of underestimation, the overall accuracy is acceptable, especially the estimated results in this study are more advantageous in terms of temporal changes.

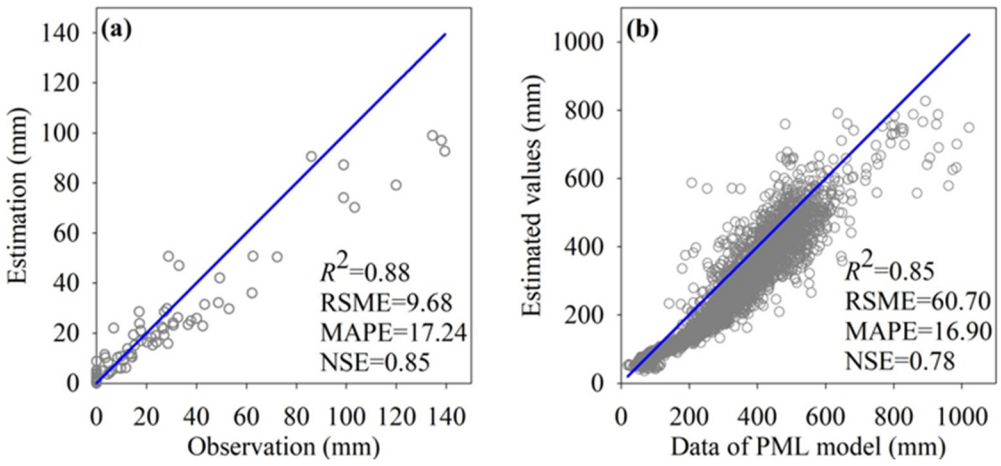

Figure A1. Validation of the *ET* data estimated using the modified Priestley–Taylor algorithm based on the MODIS remote sensing dataset. Panel (**a**) is the scatter plot between the estimated and measured monthly *ET* in two flux sites (Akesu and Fukang sites). Panel (**b**) is a scatter plot of the annual *ET* data estimated in the study and PML_V2 model which was downloaded from the National Tibetan Plateau Data Center (DOI: 10.11888/Geogra.tpdc.270251; CSTR: 18406.11.Geogra.tpdc.270251).

b. Contribution rate of human activities and climate factors to NDVI

Vegetation changes are affected by climate factors and human activities (land use changes). Therefore, human activities not only directly affect *ET*, but also indirectly affect *ET* by affecting *NDVI*. Therefore, further decomposition of vegetation and human activity coupling factors (*VH*) is required.

In bare land or extremely sparse vegetation areas, the coupling factor between vegetation and human activities (*VH*) should be dominated by human activities. In these areas,

human activities affect groundwater processes and soil hydrological processes by altering surface runoff processes, pumping groundwater, or farmland irrigation and drainage, thereby affecting *ET* processes. Here, we set the proportion of $ET_s/ET > 90\%$ to represent this area, and define the following discrimination rules:

$$\begin{cases} \varepsilon_h = \varepsilon_{vh},\ \varepsilon_{ndvi} = 0 \qquad ET_s > 0.9 \times ET \\ \varepsilon_h = \varepsilon_{h\_ndvi} \times \varepsilon_{vh},\ \varepsilon_{ndvi} = \varepsilon_{vh} - \varepsilon_h \ ET_s \le 0.9 \times ET \end{cases} \tag{A2}$$

where ε_h represents the contribution rate of human activities to *ET*; ε_{ndvi} is the contribution rate of vegetation elements to *ET*; ε_{vh} is the contribution rate of coupled elements of vegetation and human activities to *ET*; ε_{h_ndvi} represents the contribution rate of human activities to *NDVI*.

The impact of human activities on *NDVI* can be expressed as:

$$\Delta NDVI = \Delta NDVI_{\mathrm{t}} + \Delta NDVI_{\mathrm{p}} + \Delta ET_{\mathrm{hum}} \tag{A3}$$

where $\Delta NDVI_{\mathrm{t}}$, $\Delta NDVI_{\mathrm{p}}$, and $\Delta NDVI_{\mathrm{hum}}$ represent the influence of air temperature, precipitation, and human activities on *NDVI*, respectively. $\Delta NDVI$ is the variability of the average annual *NDVI* over many years, which can be expressed with its linear trend. The relationship between annual *NDVI* and climatic factors can be fitted by the following linear regression:

$$NDVI = a' \times \mathrm{T} + b' \times P + c' \tag{A4}$$

The following formula can be deduced from the Equation (A4):

$$\Delta NDVI_{\mathrm{t}} = a' \times T_{slope} \tag{A5}$$

$$\Delta NDVI_{\mathrm{p}} = b' \times P_{slope} \tag{A6}$$

$$\Delta NDVI_{\mathrm{h}} = \Delta NDVI - \Delta NDVI_{\mathrm{t}} - \Delta NDVI_{\mathrm{p}} \tag{A7}$$

Thus, the contribution rate of human activities on *NDVI* expressed as:

$$\varepsilon_{h\_ndvi} = {}^{\Delta NDVI_{\mathrm{h}}}/_{(|\Delta NDVI_{\mathrm{t}}| + |\Delta NDVI_{\mathrm{p}}| + |\Delta NDVI_{\mathrm{h}}|)} \times 100\% \tag{A8}$$

References

1. Liu, B.; Henderson, M.; Zhang, Y.; Ming, X. Spatiotemporal change in China's climatic growing season: 1955–2000. *Clim. Chang.* **2010**, *99*, 93–118. [CrossRef]
2. Hajimirzajan, A.; Vahdat, M.; Sadegheih, A.; Shadkam, E.; Bilali, H.E. An integrated strategic framework for large-scale crop planning: Sustainable climate-smart crop planning and agri-food supply chain management. *Sustain. Prod. Consum.* **2020**, *26*, 709–732. [CrossRef]
3. Peng, Y. Possible Underlying Mechanisms of Severe Decadal Droughts in Arid Central Asia During the Last 530 Years: Results From the Last Millennium Climate Reanalysis Project Version 2.0. *J. Geophys. Res. Atmos.* **2021**, *126*, e2020JD033409. [CrossRef]
4. Khaydar, D.; Chen, X.; Huang, Y.; Ilkhom, M.; Liu, T.; Friday, O.; Farkhod, A.; Khusen, G.; Gulkaiyr, O. Investigation of crop evapotranspiration and irrigation water requirement in the lower Amu Darya River Basin, Central Asia. *J. Arid. Land* **2021**, *13*, 17. [CrossRef]
5. Li, T.; Xia, J.; Zhang, L.; She, D.; Wang, G.; Cheng, L. An improved complementary relationship for estimating evapotranspiration attributed to climate change and revegetation in the Loess Plateau, China. *J. Hydrol.* **2021**, *592*, 125516. [CrossRef]
6. Yang, L.; Feng, Q.; Zhu, M.; Wang, L.; Alizadeh, M.R.; Adamowski, J.F.; Wen, X.; Yin, Z. Variation in actual evapotranspiration and its ties to climate change and vegetation dynamics in northwest China. *J. Hydrol.* **2022**, *607*, 127533. [CrossRef]
7. Banerjee, S.; Biswas, B. Assessing Climate Change Impact on Future Reference Evapotranspiration Pattern of West Bengal, India. *Agric. Sci.* **2020**, *11*, 793–802. [CrossRef]
8. Zhu, G.F.; Zhang, K.; Li, X.; Liu, S.M.; Ding, Z.Y.; Ma, J.Z.; Huang, C.L.; Han, T.; He, J.H. Evaluating the complementary relationship for estimating evapotranspiration using the multi-site data across north China. *Agric. For. Meteorol.* **2016**, *230–231*, 33–44. [CrossRef]

9. Sánchez, J.M.; López-Urrea, R.; Valentín, F.; Caselles, V.; Galve, J.M. Lysimeter assessment of the Simplified Two-Source Energy Balance model and eddy covariance system to estimate vineyard evapotranspiration. *Agric. For. Meteorol.* **2019**, *274*, 172–183. [CrossRef]
10. Luan, P.V.; Eugenio, F.C.; Filgueiras, R.; Cunha, F.; Mantovani, E.C. Mapping within-field variability of soybean evapotranspiration and crop coefficient using the Earth Engine Evaporation Flux (EEFlux) application. *PLoS ONE* **2020**, *15*, e0235620.
11. Marin, F.R.; Angelocci, L.R.; Nassif, D.; Vianna, M.S.; Carvalho, K.S. Revisiting the crop coefficient-reference evapotranspiration procedure for improving irrigation management. *Theor. Appl. Climatol.* **2019**, *138*, 1785–1793. [CrossRef]
12. Paciolla, N.; Corbari, C.; Hu, G.; Zheng, C.; Mancini, M. Evapotranspiration estimates from an energy-water-balance model calibrated on satellite land surface temperature over the Heihe basin. *J. Arid. Environ.* **2021**, *188*, 104466. [CrossRef]
13. Denager, T.; Looms, M.C.; Sonnenborg, T.O.; Jensen, K.H. Comparison of evapotranspiration estimates using the water balance and the eddy covariance methods. *Vadose Zone J.* **2020**, *19*. [CrossRef]
14. Elkatoury, A.; Alazba, A.A.; Mossad, A. Estimating Evapotranspiration Using Coupled Remote Sensing and Three SEB Models in an Arid Region. *Environ. Process.* **2020**, *7*, 109–133. [CrossRef]
15. Senkondo, W.; Munishi, S.E.; Tumbo, M.; Nobert, J.; Lyon, S.W. Comparing Remotely-Sensed Surface Energy Balance Evapotranspiration Estimates in Heterogeneous and Data-Limited Regions: A Case Study of Tanzania's Kilombero Valley. *Remote Sens.* **2019**, *11*, 1289. [CrossRef]
16. Yao, Y.J.; Liang, S.L.; Zhou, G.Y.; Li, Y.L. MODIS-driven estimation of terrestrial latent heat flux in China based on a modified Priestley–Taylor algorithm. *Agric. For. Meteorol.* **2013**, *171–172*, 187–202. [CrossRef]
17. Brutsaert, W. A generalized complementary principle with physical constraints for land-surface evaporation. *Water Resour. Res.* **2016**, *51*, 8087–8093. [CrossRef]
18. Feng, S.; Liu, J.; Zhang, Q.; Zhang, Y.; Sun, P. A global quantitation of factors affecting evapotranspiration variability. *J. Hydrol.* **2020**, *584*, 124688. [CrossRef]
19. Ning, T.; Li, Z.; Feng, Q.; Qin, Y. Attribution of growing season evapotranspiration variability considering snowmelt and vegetation changes in the arid alpine basins. *Hydrol. Earth Syst. Sci.* **2021**, *25*, 3455–3469. [CrossRef]
20. Hu, S.; Mo, X. Attribution of Long-Term Evapotranspiration Trends in the Mekong River Basin with a Remote Sensing-Based Process Model. *Remote Sens.* **2021**, *13*, 303. [CrossRef]
21. Hu, Z.; Zhang, C.; Hu, Q.; Tian, H. Temperature Changes in Central Asia from 1979 to 2011 Based on Multiple Datasets. *J. Clim.* **2014**, *27*, 1143–1167. [CrossRef]
22. Zhu, X.; Wei, Z.; Dong, W.; Ji, Z.; Chen, D. Dynamical downscaling simulation and projection for mean and extreme temperature and precipitation over central Asia. *Clim. Dyn.* **2020**, *54*, 3279–3306. [CrossRef]
23. Hao, X.; Chen, Y.; Xu, C.; Li, W. Impacts of Climate Change and Human Activities on the Surface Runoff in the Tarim River Basin over the Last Fifty Years. *Water Resour. Manag.* **2008**, *22*, 1159–1171. [CrossRef]
24. Su, Y.; Li, X.; Feng, M.; Nian, Y.; Huang, L.; Xie, T.; Zhang, K.; Chen, F.; Huang, W.; Chen, J. High agricultural water consumption led to the continued shrinkage of the Aral Sea during 1992–2015. *Sci. Total Environ.* **2021**, *777*, 145993. [CrossRef] [PubMed]
25. Deliry, S.I.; Avdan, Z.Y.; Do, N.T.; Avdan, U. Assessment of human-induced environmental disaster in the Aral Sea using Landsat satellite images. *Environ. Earth Sci.* **2020**, *79*, 471. [CrossRef]
26. Chen, F.-H.; Chen, J.-H.; Holmes, J.; Boomer, I.; Austin, P.; Gates, J.B.; Wang, N.-L.; Brooks, S.J.; Zhang, J.-W. Moisture changes over the last millennium in arid central Asia: A review, synthesis and comparison with monsoon region. *Quat. Sci. Rev.* **2010**, *29*, 1055–1068. [CrossRef]
27. Li, Z.; Chen, Y.; Fang, G.; Li, Y. Multivariate assessment and attribution of droughts in Central Asia. *Sci. Rep.* **2017**, *7*, 1316. [CrossRef]
28. Chen, H.; Liu, H.; Chen, X.; Qiao, Y. Analysis on impacts of hydro-climatic changes and human activities on available water changes in Central Asia. *Sci. Total Environ.* **2020**, *737*, 139779. [CrossRef]
29. Zeng, Z.; Piao, S.; Li, L.Z.X.; Zhou, L.; Ciais, P.; Wang, T.; Li, Y.; Lian, X.; Wood, E.F.; Friedlingstein, P.; et al. Climate mitigation from vegetation biophysical feedbacks during the past three decades. *Nat. Clim. Change* **2017**, *7*, 432–436. [CrossRef]
30. Hao, X.; Zhang, S.; Li, W.; Duan, W.; Fang, G.; Ying, Z.; Guo, B. The Uncertainty of Penman-Monteith Method and the Energy Balance Closure Problem. *J. Geophys. Res. Atmos.* **2018**, *123*, 7433–7443. [CrossRef]
31. Allen, R.G. Crop Evapotranspiration-Guidelines for computing crop water requirements. *FAO Irrig. Drain. Pap. (FAO)* **1998**, *56*, D05109.
32. Ullah, S.; You, Q.; Ullah, W.; Ali, A. Observed changes in precipitation in China-Pakistan economic corridor during 1980–2016. *Atmos. Res.* **2018**, *210*, 1–14. [CrossRef]
33. Arrieta-Castro, M.; Donado-Rodríguez, A.; Acua, G.J.; Canales, F.A.; Kamierczak, B. Analysis of Streamflow Variability and Trends in the Meta River, Colombia. *Water* **2020**, *12*, 1451. [CrossRef]
34. Zhang, D.; Liu, X.; Zhang, L.; Zhang, Q.; Gan, R.; Li, X. Attribution of Evapotranspiration Changes in Humid Regions of China from 1982 to 2016. *J. Geophys. Res. Atmos.* **2020**, *125*, 1451. [CrossRef]
35. Li, Z.; Chen, Y.; Yang, J.; Wang, Y. Potential evapotranspiration and its attribution over the past 50years in the arid region of Northwest China. *Hydrol. Process.* **2014**, *28*, 1025–1031. [CrossRef]
36. Vadeboncoeur, M.A.; Green, M.B.; Heidi, A.; Campbell, J.L.; Beth, A.M.; Boyer, E.W.; Burns, D.A.; Fernandez, I.J.; Mitchell, M.J.; Shanley, J.B. Systematic variation in evapotranspiration trends and drivers across the Northeastern United States. *Hydrol. Process.* **2018**, *32*, 3547–3560. [CrossRef]

37. Hu, D.; Xu, M.; Kang, S.; Wu, H. Impacts of climate change and human activities on runoff changes in the Ob River Basin of the Arctic region from 1980 to 2017. *Theor. Appl. Climatol.* **2022**, *148*, 1663–1674. [CrossRef]
38. Wang, Y.; Gu, X.; Yang, G.; Yao, J.; Liao, N. Impacts of climate change and human activities on water resources in the Ebinur Lake Basin, Northwest China. *J. Arid. Land* **2021**, *13*, 18. [CrossRef]
39. Zhou, H.; Chen, Y.; Hao, X.; Zhao, Y.; Fang, G.; Yang, Y. Tree rings: A key ecological indicator for reconstruction of groundwater depth in the lower Tarim River, Northwest China. *Ecohydrology* **2019**, *12*, e2142. [CrossRef]
40. Hao, X.; Li, W. Impacts of ecological water conveyance on groundwater dynamics and vegetation recovery in the lower reaches of the Tarim River in northwest China. *Environ. Monit. Assess.* **2014**, *186*, 7605. [CrossRef]
41. Chen, H.; Zhang, W.; Shalamzari, M.J. Remote detection of human-induced evapotranspiration in a regional system experiencing increased anthropogenic demands and extreme climatic variability. *Int. J. Remote Sens.* **2019**, *40*, 1887–1908. [CrossRef]
42. Zou, M.; Niu, J.; Kang, S.; Li, X.; Lu, H. The contribution of human agricultural activities to increasing evapotranspiration is significantly greater than climate change effect over Heihe agricultural region. *Sci. Rep.* **2017**, *7*, 8805. [CrossRef]
43. Wu, Y. Impacts of Human Activities on the Variations in Terrestrial Water Storage of the Aral Sea Basin. *Remote Sens.* **2021**, *13*.
44. Yang, P.; Xia, J.; Zhan, C.; Chen, X.; Qiao, Y.; Chen, J. Separating the impacts of climate change and human activities on actual evapotranspiration in Aksu River Basin ecosystems, Northwest China. *Nord. Hydrol.* **2018**, *49*, 1740–1752. [CrossRef]
45. Li, W.; Huang, F.; Shi, F.; Wei, X.; Zamanian, K.; Zhao, X. Human and climatic drivers of land and water use from 1997 to 2019 in Tarim River basin, China. *Int. Soil Water Conserv. Res.* **2021**, *9*, 532–543. [CrossRef]
46. Zhao, Y.; Xue, J.; Wu, N.; Hill, R.L. An Artificial Oasis in a Deadly Desert: Practices and Enlightenments. *Water* **2022**, *14*, 2237. [CrossRef]
47. Du, Q.; Zhang, M.; Wang, S.; Che, C.; Rong, M.; Ma, Z. Changes in air temperature over China in response to the recent global warming hiatus. *J. Geogr. Sci.* **2019**, *29*, 21. [CrossRef]
48. Dong, Q.; Wang, W.; Shao, Q.; Xing, W.; Ding, Y.; Fu, J. The response of reference evapotranspiration to climate change in Xinjiang, China: Historical changes, driving forces, and future projections. *Int. J. Climatol.* **2020**, *40*, 235–254. [CrossRef]
49. Fisher, J.B.; Tu, K.P.; Baldocchi, D.D. Global estimates of the land–atmosphere water flux based on monthly AVHRR and ISLSCP-II data, validated at 16 FLUXNET sites. *Remote Sens. Environ.* **2008**, *112*, 901–919. [CrossRef]
50. Cao, M.; Wang, W.; Xing, W.; Wei, J.; Chen, X.; Li, J.; Shao, Q. Multiple sources of uncertainties in satellite retrieval of terrestrial actual evapotranspiration. *J. Hydrol.* **2021**, *601*, 126642. [CrossRef]
51. Mu, Q.; Zhao, M.; Running, S.W. Improvements to a MODIS global terrestrial evapotranspiration algorithm. *Remote Sens. Environ.* **2011**, *115*, 1781–1800. [CrossRef]
52. Zhang, Y.; Leuning, R.; Hutley, L.B.; Beringer, J.; McHugh, I.; Walker, J.P. Using long-term water balances to parameterize surface conductances and calculate evaporation at 0.05 spatial resolution. *Water Resour. Res.* **2010**, *46*, 5. [CrossRef]
53. Zhang, Y. PML_V2 Global Evapotranspiration and Gross Primary Production (2002.07–2019.08). National Tibetan Plateau/Third Pole Environment Data Center. 2020. Available online: https://data.tpdc.ac.cn/en/data/48c16a8d-d307-4973-abab-972e9449627c/ (accessed on 26 October 2022).
54. Zhang, Y.; Kong, D.; Gan, R.; Chiew, F.H.; McVicar, T.R.; Zhang, Q.; Yang, Y. Coupled estimation of 500 m and 8-day resolution global evapotranspiration and gross primary production in 2002–2017. *Remote Sens. Environ.* **2019**, *222*, 165–182. [CrossRef]